Isı Bilimi ve Tekniği Dergisi, 40, 1, 15-25, 2020
J. of Thermal Science and Technology
©2020 TIBTD Printed in Turkey
ISSN 1300-3615

THE EFFECTS OF CO_2, H_2O, AND N_2 DILUTIONS ON POLLUTANTS OF SHALE GAS COMBUSTION

Suat ÖZTÜRK
Zonguldak Bülent Ecevit University, Zonguldak Vocational School, Department of Electronic and Automation
67100 Merkez, Zonguldak, suatozturk@beun.edu.tr

(Geliş Tarihi: 19.03.2019, Kabul Tarihi: 03.12.2019)

Abstract: Increase in demands for energy and discovered huge reserves of shale gas in the world cause countries and researchers to focus on it progressively. The amount of shale gas production has begun to rise by developing the techniques of gas extraction from shale rocks recently. In this paper, the non-premixed combustion characteristic and emissions of shale gas and humid air with dilution effects are numerically investigated under different equivalence ratio, pressure and temperature. A two dimension model of cylindrical combustor is considered. It is concluded that NO_x for New Albany and Haynesville come to the maximum value at 1.025 and 1.02 of equivalence ratio and the maximum reaction temperatures are 2027 and 2014 K in turn. The rising equivalence ratio raises CO mass fractions. The increasing dilution rates decrease NO_x and uplift CO mass fractions. The enhancing pressure rears NO_x and diminishes CO fractions. The ascending wall temperature boosts NO_x, CO and reaction temperatures. NO_x and CO from environmental pollutants emerging at the end of shale gas combustion can be lowered by decreasing equivalence ratio, wall temperature, and pressure. The use of H_2O dilution steps forward in compared with CO_2 and N_2 because of its opposite effects on NO_x and CO pollutants.
Keywords: Shale gas, Non-premixed combustion, Turbulent, Nitrogen oxides.

ŞEYL GAZ YANMASININ KİRLETİCİLERİ ÜZERİNDE CO_2, H_2O VE N_2 DİLÜSYONLARININ ETKİLERİ

Özet: Dünyada şeyl gazın keşfedilmiş büyük rezervleri ve enerji taleplerindeki artış, ülkelerin ve araştırmacıların artan bir şekilde şeyl gaz üzerine odaklanmasına sebep olmaktadır. Şeyl gazın üretim miktarı, son zamanlarda şeyl kayalarından gazın çıkartılması tekniklerinin geliştirilmesi ile artmaya başladı. Bu çalışmada, dilüsyon etkileri ile birlikte şeyl gaz ve nemli havanın ön karışımsız yanma karakteristikleri ve emisyonları, farklı ekivalans oranları, basınç ve sıcaklıklar altında sayısal olarak araştırılmıştır. Silindiriksel yakıcının iki boyutlu bir modeli düşünülmüştür. New Albany ve Haynesville için NO_x'lerin, 1.025 ve 1.02 ekivalans oranında maksimum değere ulaştığı ve maksimum reaksiyon sıcaklıklarının sırasıyla 2027 ve 2014 K olduğu sonucuna varılmıştır. Artan ekivalans oranı CO kütle kesitlerini yükseltmektedir. Yükselen dilüsyon oranları NO_x'i düşürmekte ve CO kütle kesitlerini artırmaktadır. Artan basınç NO_x'i yükseltmekte ve CO kesitlerini azaltmaktadır. Yükselen duvar sıcaklığı NO_x, CO ve reaksiyon sıcaklıklarını artırmaktadır. Şeyl gaz yanmasının sonunda ortaya çıkan çevresel kirleticilerden NO_x ve CO, ekivalans oranı, duvar sıcaklığı ve basıncı düşürerek azaltılabilir. CO_2 ve N_2 ile karşılaştırıldığında, NO_x ve CO kirleticileri üzerindeki zıt etkilerinden dolayı H_2O dilüsyonunun kullanımı bir adım öne çıkmaktadır.
Anahtar Kelimeler: Şeyl gazı, Ön karışımsız yanma, Türbülans, Nitrojen oksitler.

NOMENCLATURE

CFD	Computational fluid dynamics
CH_4	Methane
C_2H_6	Ethane
C_3H_8	Propane
CO	Carbon monoxide
CO_2	Carbon dioxide
N_2	Nitrogen
NO_x	Nitrogen oxides
NO	Nitrogen monoxide
NO_2	Nitrogen dioxide
A_k	Surface area [m^2]
K	Thermal conductivity [W/m.K]
MM	Molecular mass [kg/mol]
Pr	Prandtl number [=$\mu.c_p/k$]
R	Gas constant [J/mol.K]
S_{rea}, S_{rad}	Thermal energy causing by chemical reactions and radiative transfer [J]
T_{wall}	Wall temperature [K]
c_p	Specific heat [J/kg.K]
f_x	Mass fraction [kg x/kg]
h	Enthalphy [J/mol]
k,ε	Turbulent kinetic energy and its dissipation
u, v	Axial and radial velocities [m/s]
σ	Stefan-Boltzman constant

ρ Specific mass [kg/m^3]
μ Dynamic viscosity [kg.m/s]

INTRODUCTION

Hydro carbon based fuels still take an important place at the electricity and energy production for the purposes of heating and cooling, lighting, transporting, communication, sanitation, etc. Many countries seek out alternatives emitting lower greenhouse gases for differentiating energy sources. Shale gas as a new energy source comes forward with the confirmed potential of countries in the last years (Cohen and Winkler, 2014; Chang et al., 2015). The total shale gas reserve in the world is 214.5 trillion cubic meters by 1.4 times of natural gas. China, Argentina, Algeria, USA, Canada, Mexico, Australia, South Africa are among countries possessing crucial shale gas reserves (Lan et al., 2019).

Shale gas reservoirs have organic-rich deposition, low matrix permeability, and mineral-filled nature fracture clusters. It has a better production cycle and long mining life according to natural gas as well (Bilgen and Sarıkaya, 2016; Wang et al., 2019). United States firstly extracted by horizontal drilling and hydraulic fracturing procedures and currently sells it commercially. The water pollution and earthquakes caused by hydraulic fracturing process and greenhouse gases emitted by fugitive methane seem as environmental issues to be solved at shale gas extraction (Wang et al., 2014).

Electricity production from shale gas is realized by the combustion process in energy plants. Shale gas burned by air emits various hazardous emissions. Nitrogen oxides (NO_x) and carbon monoxide (CO) are seen as the most unfavorable and obtrusive environmental pollutants emerging at the end of shale gas combustion because of fuel and oxide ingredients, high reaction temperature, and incomplete combustion. NO_x causes for respiratory illness, acid rains, and smog. CO is a toxic gas poisoning the living things (Akça et al., 2017; Alberts, 1994). NO_x comes to exist by the oxidation of nitrogen and oxygen in three ways called thermal, prompt, and fuel NO_x depending on stoichiometry, reaction temperature, and nitrogen concentration in fuel and air. Thermal way transcends more at the reaction temperatures above 1300 ºC. CO occurs by the reaction of carbon and oxygen during the incomplete combustion (Ozturk, 2018).

The combustion case of gas and other fuels in various types of combustors are both numerically and experimentally examined under different conditions as turbulent, laminar, adiabatic, non-adiabatic, premixed, non-premixed, partially premixed, and etc. Studies for shale gases in literature have mostly focused on the environmental effects of the extracting process of shale gas. It is seen that there is a gap for the combustion process, characteristics, and emissions of shale gas. Cohen and Winkler (2014) concluded shale gas have lower greenhouse gas emissions with respect to coal for the electricity generation. Chang et al. (2015) determined the greenhouse gas emissions of shale gas fired electricity are lower than those of coal. Ozturk (2018) detected that rising inlet pressure increases NO_x, accruing humidity ratio decreases NO_x, and growing flow rate diminishes NO_x for non-premixed shale gas combustion. Vargas et al. (2016) detected the shale gas consisting of 58% CH_4 - 20% C_2H_6 - 12% C_3H_8 - 10% CO_2 indicates higher laminar burning velocity than the others. Zahedi and Yousefi (2014) indicated the addition of N_2 or CO_2 to the mixture reduces NO and the rising initial pressure arises NO in pre-mixed laminar methane-air combustion. McTaggart-Cowan et al. (2009) found that nitrogen addition lowers NO_x emissions and ethane addition enhances it in high-pressure non-premixed natural gas combustion. Jerzak et al. (2014) proved that CO_2 addition to natural gas increases CO and causes to NO_x and the combustion temperature to decrease. Silva et al. (2007) studied on CO and CO_2 emissions and temperature distributions for turbulent non-premixed combustion of natural gas in a cylindrical chamber. Hayashi et al. (1998) determined NO_x rises with pressure and temperature increment in non-premixed gas combustion.

In this study, the temperature and emission characteristics of turbulent, non-premixed and non-adiabatic combustion of shale gas and humid air in a cylindrical combustor are computationally investigated under the dilutive effects of CO_2, H_2O, and N_2 added in the burning air by ANSYS software.

MATHEMATICAL FORMULATION

The CFD simulation of shale gas and humid air combustion in a cylindrical burner is the calculations of heat and mass transfer, chemical species concentration and velocities, temperatures, and thermal radiation equations defining the combustion process with finite rates chemical reactions.

Mass Conservation

The continuity equation for cylindrical coordinates is given by

$$\frac{\partial}{\partial x}\rho\bar{u} + \frac{\partial}{\partial r}\rho\bar{v} + \frac{\rho\bar{v}}{r} = 0 \quad (1)$$

where $\bar{u}$ and $\bar{v}$ are time averaged velocities, ρ is the specific mass of the mixture, and x and r are the axial and radial coordinates.

Momentum Conservation

The flow equations in axial and radial directions can be written by

$$\bar{u}\frac{\partial}{\partial x}(\rho\bar{u})+\bar{v}\frac{\partial}{\partial r}(\rho\bar{u})=-\frac{\partial p^{*}}{\partial x}+\vec{\nabla}.((\mu+\mu_t)\vec{\nabla}\bar{u})+\frac{\partial}{\partial x}\left(\mu_t\frac{\partial\bar{u}}{\partial x}\right)+\frac{1}{r}\frac{\partial}{\partial r}\left(r\mu_t\frac{\partial\bar{v}}{\partial x}\right) \quad (2)$$

$$\bar{u}\frac{\partial}{\partial x}(\rho\bar{v})+\bar{v}\frac{\partial}{\partial r}(\rho\bar{v})=-\frac{\partial p^{*}}{\partial r}+\vec{\nabla}.((\mu+\mu_t)\vec{\nabla}\bar{v})+\frac{\partial}{\partial x}\left(r\mu_t\frac{\partial\bar{u}}{\partial r}\right)+\frac{1}{r}\frac{\partial}{\partial r}\left(r\mu_t\frac{\partial\bar{v}}{\partial r}\right)-\frac{(\mu+\mu_t)\bar{v}}{r^2}+\frac{\rho\bar{w}^2}{r} \quad (3)$$

$$\mu_t=C_\mu\rho\frac{k^2}{\varepsilon} \quad (4)$$

$$p^{*}=\bar{p}-\left(\frac{2}{3}\right)k \quad (5)$$

where μ and μ_t are mixture dynamic and turbulent viscosity, p and p^* is time averaged and modified pressures, and C_μ, k and ε are an empirical constant for the turbulent model, the turbulent kinetic energy and its dissipation respectively.

The k-ε Turbulence Model

The equations for k and ε where σ_k, σ_ε, $C_{1,\varepsilon}$,$C_{2,\varepsilon}$ and P_k are Prandtl numbers for kinetic energy and dissipation, empirical constants of turbulent model and the destruction or production of turbulent kinetic energy is given as

$$\bar{u}\frac{\partial}{\partial x}(\rho k)+\bar{v}\frac{\partial}{\partial r}(\rho k)=\vec{\nabla}.\left(\left(\mu+\frac{\mu_t}{\sigma_k}\right)\vec{\nabla}k\right)+P_k-\rho\varepsilon \quad (6)$$

$$\bar{u}\frac{\partial}{\partial x}(\rho\varepsilon)+\bar{v}\frac{\partial}{\partial r}(\rho\varepsilon)=\vec{\nabla}.\left(\left(\mu+\frac{\mu_t}{\sigma_\varepsilon}\right)\vec{\nabla}\varepsilon\right)+C_{1,\varepsilon}\frac{\varepsilon}{k}P_k-C_{2,\varepsilon}\frac{\varepsilon^2}{k} \quad (7)$$

$$P_k=\mu_t\left(2\left(\frac{\partial\bar{u}}{\partial x}\right)^2+\left(\frac{\partial\bar{u}}{\partial r}+\frac{\partial\bar{v}}{\partial x}\right)^2\right)+\mu_t\left(2\left(\frac{\partial\bar{v}}{\partial r}\right)^2+2\left(\frac{\bar{v}}{r}\right)^2\right) \quad (8)$$

Energy Conservation

The energy equation by neglecting the transport of energy can be written as

$$\bar{u}\frac{\partial}{\partial x}(\rho\bar{h})+\bar{v}\frac{\partial}{\partial r}(\rho\bar{h})=\vec{\nabla}.\left(\left(\frac{K}{c_p}+\frac{\mu_t}{\mathrm{Pr}_t}\right)\vec{\nabla}\bar{h}\right)+\bar{S}_{rad}+\bar{S}_{rea} \quad (9)$$

$$c_p=\sum\nolimits_x\bar{f}_x c_{p,x} \quad (10)$$

$$\bar{S}_{rea}=\sum\nolimits_x\left(\frac{h_x^o}{\overline{MM}_x}+\int_{\bar{T}_{ref,x}}^{\bar{T}}c_{p,x}d\bar{T}\right)\bar{R}_x \quad (11)$$

$$\bar{S}_{rad,k}=\frac{1}{A_k}\left(\sum\nolimits_{\gamma=1}^{\Gamma}\vec{g}_\gamma\vec{s}_k\sigma\bar{T}_\gamma^{\,4}+\sum_{j=1}^{J}\vec{s}_j\vec{s}_k q_{o,j}\right)-q_{o,k} \quad (12)$$

where h and c_p are average enthalpy and specific heat, $c_{p,x}$, f_x, MM_x, Pr_t, K and are specific heat, average mass fraction, and mixture molecular mass of x-th chemical specie, turbulent Prandtl number, and thermal conductivity of mixture, S_{rea} and S_{rad} are the sources of thermal energy causing by chemical reactions and radiative transfer, A_k is surface area, σ are Stefan-Boltzman constant, and $g_\gamma s_k$ and $s_j s_k$ are directed-flux areas (Silva et al., 2007).

MATERIALS AND METHODS

The combustion issue is a complex process based on fluid mechanics, heat and mass transfer, chemical kinetics, thermos dynamics, radiation, and etc. Researchers mostly prefer numerical solution being close to the experimental results because the experiments are hard to handle with, expensive, and need more time. The computational fluid dynamics (CFD) as a numerical method is used at the solution of combustion problems by computing temperatures, rates, mass fractions, products, and emissions under the given conditions. CFD software utilized for calculations in this study is Fluid Flow (Fluent) of ANSYS solving the equations of combustion defined by mathematical models under the selected solution methods, controls, and boundary conditions over meshed geometry of a burner chamber (Ozturk, 2018).

In ANSYS's non-premixed combustion that fuel (shale gas) and oxidizer (humid air) enter the reaction zone as seperate streams, the thermochemistry is degraded to a single parameter called the mixture fraction, f. The mixture fraction is the local mass fraction of elements (C, H, O, N, etc.) of burnt and unburnt fuel stream in all the species (N_2, CO_2, H_2O, O_2, CO, etc.) and the atomic elements are conserved in chemical reactions. In this approach, the governing transport equation of mixture fraction does not include a source term because it is a conserved scalar quantity. Thus, the case of gas combustion is reduced to a mixing problem and removes the difficulties including non-linear mean reaction rates. As a result, the chemistry is modeled as being in chemical equilibrium once mixed (ANSYS, 2009).

A 2D model of the cylindrical chamber is devised to simplify and accelerate CFD solutions. Grid independence test for the model are realized at numbers of different elements for Haynesville shale gas as given

in Figure 1. The mesh of 12000 elements and 12261 nodes for combustion field is decided to use for the computations because it provides fast solution and requires less time and energy for CFD at considering of enormous size of the cylindrical combustor. The percentage differences for reaction temperatures and mass fractions of NO_x and CO between element numbers of 12000 and 40500 are 0.8 and 6.4% respectively in acceptable limits. The meshed combustor chamber under Mesh section in ANSYS software is given in Figure 2.

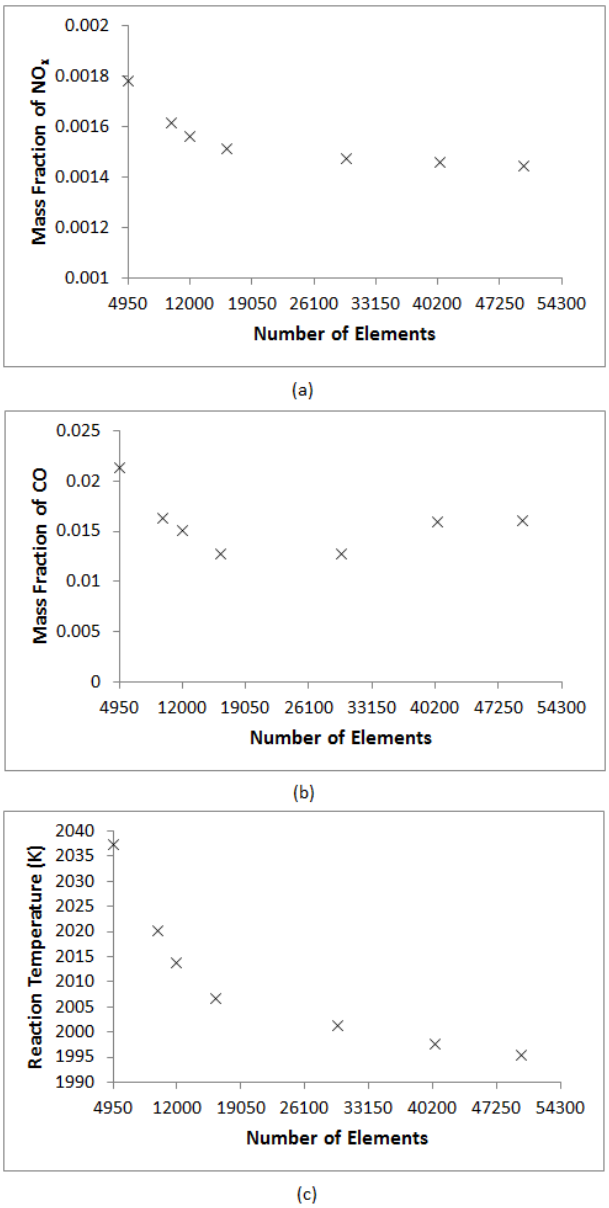

Figure 1. Grid independence test at different element numbers.

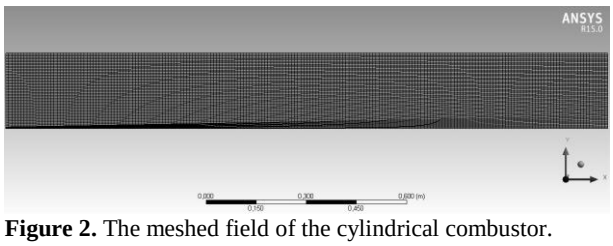

Figure 2. The meshed field of the cylindrical combustor.

The inlet flow rates, temperatures, and the dimensions of the cylindrical combustor are illustrated in Figure 3. The burning air includes onset humidity at the rate of 1.5%, the pressure is 1 Atm, the wall, inlet fuel and air temperatures are 300 K and equivalence ratio is 1 if not mentioned else in the study. The diluents of CO_2, H_2O, and N_2 to investigate the dilutive effects on the combustion characteristics are added to the burning air at different ratios between 0 and 30%.

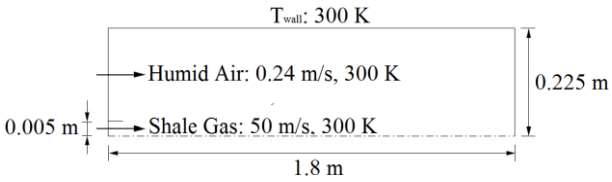

Figure 3. The temperatures and rates of fuel and oxide entering the combustor (Ozturk, 2018; ANSYS, 2009).

Shale gases used in the calculations are extracted from New Albany and Haynesville regions of United States. The average values of the compositions of the gases obtained from the fields in these regions are given in Table 1. It is seen that the compositions of shale gases aggregate around two different types because compositions of shale gases extracted at other countries generally resemble to the compositions of New Albany and Haynesville shale gases.

Table 1. The shale gas compositions (Bullin et al., 2008).

Regions	CH_4	C_2H_6	C_3H_8	CO_2	N_2
Haynesville	95	0.1	0	4.8	0.1
New Albany	89.875	1.125	1.125	7.875	0

To solve the equations of energy, k-epsilon, radiation, etc. defining the present case of gas combustion in CFD simulation needs to be assigned setup parameters in ANSYS Fluent software. Moreover, the models of turbulent, non-premixed, non-adiabatic, and NO_x also needs to be selected. Thermal and prompt NO_x formation and N_2O intermediate steps are crucial for NO_x production in gas combustion. P1 model works reasonably for radiation in combustion, facilitates radiative transfer equations, and also includes scattering effects of particles, droplets, and soot. Standard k-epsilon (2 eqn.) model generally presents enough solution for turbulent cases and decreases computational costs per iteration. Standard wall functions are widely used for mean velocity in turbulent boundary layer of industrial flows.

The following models and properties are selected from under Setup section: Energy–On, Viscous Model–k-epsilon (2 eqn.) and k-epsilon model–standard, Near-Wall Treatment–Standard Wall Functions, Radiation Model–P1, Species Model–Non-Premixed Combustion (Inlet Diffusion, Chemical Equilibrium, Non-Adiabatic are selected), NO_x Model–On (Thermal, Prompt and N_2O Intermediate are selected). The compositions of

fuel and air for the complete combustion and others at several equivalence ratios are entered under Fuel and Oxide at Boundary tab of PDF Table.

RESULTS AND DISCUSSION

Mass fractions of CH_4 and CO_2 along symmetry line are represented in Figure 4a, b. The results indicate that computed mass concentrations of combustion products have trends that are similar to those of numerical simulation (Silva et al., 2007) and experimental data (Garreton and Simonin, 1994). The fuel and air begin to combust after a certain distance because there is a dividing wall between air and fuel at the entrance of the cylindrical combustor in the present study. Mass fraction of CO_2 begins at 0.12 because Haynesville shale gas includes 4.8% CO_2.

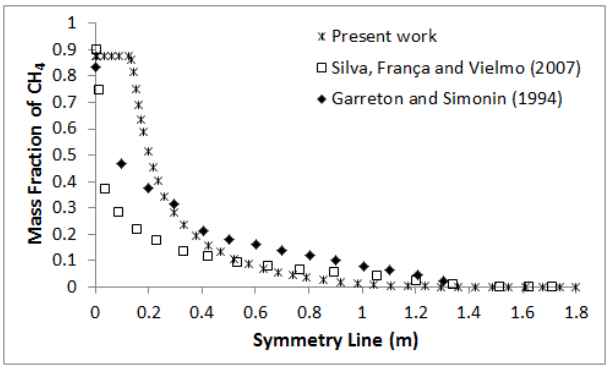

(a)

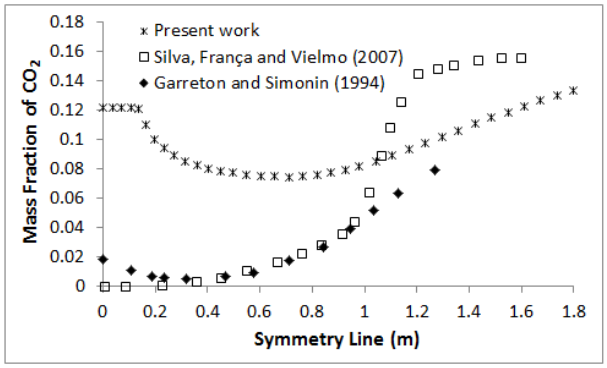

(b)

Figure 4. Mass fractions of CH_4 and CO_2 along symmetry line with numerical simulation (Silva et al., 2007) and experimental data (Garreton and Simonin, 1994).

The mass fractions of NO_x emerging at the end of non-premixed combustions of shale gases at various equivalence ratios (ER) are given in Figure 5a. NO_x reach to the maximum at 1.025 of ER as 0.0021 kg NO_x/kg for New Albany and 1.02 of ER as 0.00158 kg NO_x/kg for Haynesville. New Albany has the higher NO_x values because of its high C_2H_6 and C_3H_8 components. The difference between NO_x of gases at ER=1 is 25%. The burning air rate in the combustion chamber decreases by rising equivalence ratio and it causes the incomplete combustion. The incomplete burning leads to the fall of NO_x and reaction temperatures and the increment of CO mass fraction by enhancing carbon and hydro carbon compounds in the chamber as illustrated in Figure 5b. The difference between CO mass fractions is 24.5% at ER=1. The reaction temperatures are depicted in Figure 5c. The maximum reaction temperatures are 2027 and 2014 K for New Albany and Haynesville. It is seen that NO_x follows the reaction temperature because thermal NO_x is especially more effective than prompt and fuel NO_x at reaction temperatures above 1300 ^oC.

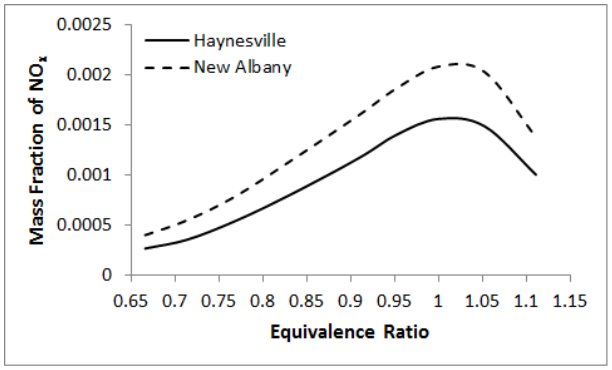

(a)

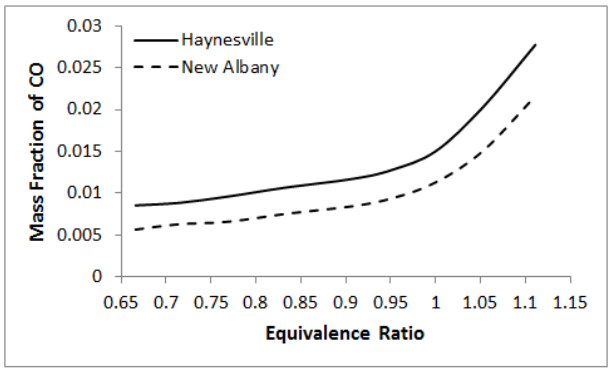

(b)

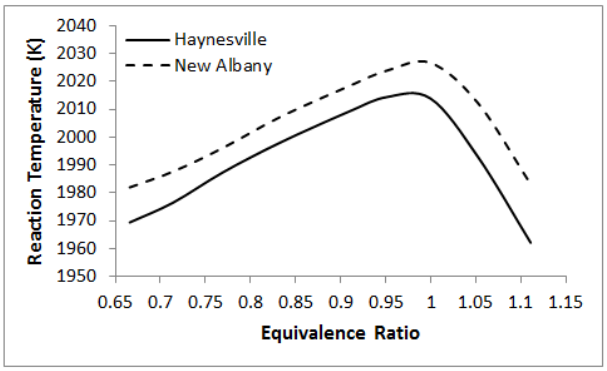

(c)

Figure 5. The reaction temperatures,NO_x and CO mass fractions of shale gases at different equivalence ratios.

The mass fractions of NO_x under the dilutive effects of CO_2, H_2O, and N_2 additions into the burning air are depictured in Figure 6a, b. The enhancing dilution rates diminish NO_x values for both shale gases. NO_x is decreased at the furthest by H_2O addition following by CO_2 and N_2. The high heat hold capacity of H_2O cushions the reaction temperature and fades NO_x. The addition of CO_2 into the air reduces the reaction temperature by dropping reaction rates, species

concentrations, and flame speed during the combustion and the decreasing flame temperature lowers NO_x (Hraiech et al., 2015). N_2 dilution causes NO to fall down because it decreases the temperature by altering the temperature based kinetic pathways (Sabia et al., 2015). 5% dilution of H_2O, CO_2, and N_2 abates NO_x 59.1, 51.3, and 51.2% for Haynesville and 57.2, 49.3, and 49.1% for New Albany respectively.

The dilution additions cause CO mass fractions to increase for all the shale gas as given in Figure 6c, d. As expected, CO_2 addition enhances CO mass fraction at the highest rate by raising carbon atoms in the burning chamber. H_2O dilution has the least effect for CO emissions to rise. 5% addition of H_2O, N_2, and CO_2 increases CO mass fractions 30.1, 45.2, and 61.9% for Haynesville and 32.8, 50.3, and 62.4% for New Albany.

The reaction temperatures are represented in Figure 6e, f. The excessive decrease in reaction temperature is an unfavorable situation from the view point of system output. The rank from highest to the lowest for dilutions to reduce the reaction temperature is CO_2, H_2O, and N_2 respectively. 5% addition of CO_2, H_2O, and N_2 into the air falls the temperatures down 5.1, 4.2, and 3.6% for Haynesville and 4.8, 3.8, and 3.25% for New Albany. It can be interpreted that H_2O dilution indicates the best effects under the evaluations of NO_x, CO emissions and reaction temperatures.

Figure 7a and b illustrates NO_x mass fractions for Haynesville and New Albany shale gases at 10% dilutions of CO_2, H_2O, and N_2 under different pressures.

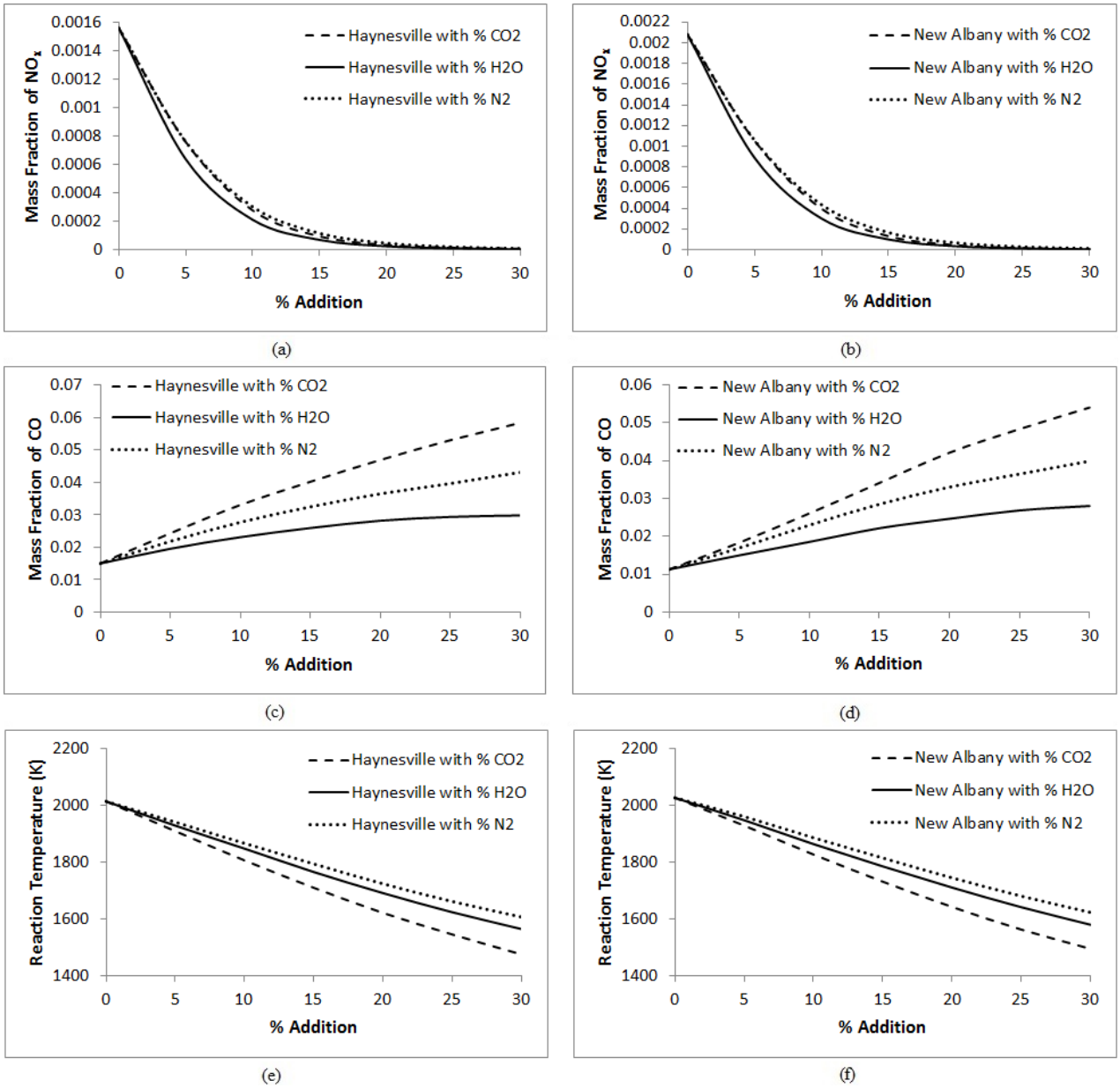

Figure 6. The mass fraction and reaction temperatures of shale gases at various dilution rates: (a) NO_x mass fractions for Haynesville, (b) NO_x mass fractions for New Albany, (c) CO mass fractions for Haynesville, (d) CO mass fractions for New Albany, (e) Reaction temperatures for Haynesville, and (f) Reaction temperatures for New Albany shale gas.

The pressure is absolute. The rising pressure raises NO_x values for both gases. The highest values for NO_x occur with N_2 dilution followed by CO_2 and H_2O in the decreasing range. The variances between 0 and 10 Atm with N_2, CO_2, and H_2O additions are 317, 258, and 327% for Haynesville and 292, 239, and 302% for New Albany. The highest increment of NO_x at the interval of 0-10 Atm belongs to H_2O dilution.

CO emissions are depicted in Figure 7c and d. CO mass fractions reduce up to 2 Atm and stay constant between 2 and 10 Atm. The high pressure reduces CO because the necessary time for the reaction of carbon and oxygen atoms is not available (Muharam et al., 2015). The highest CO values arise with CO_2 dilution pursued by N_2 and H_2O additions. The decrease rates for CO between 0 and 2 Atm in the rank of CO_2, N_2, and H_2O are 12.9, 11.9, and 10.1% for Haynesville and 14.9, 17.3, and 14.1% for New Albany.

The enhancing pressure increases the reaction temperatures as shown in Figure 7d and e. The rising pressure shortens the flame length, the reactions occur in a micro area, and the fuel is depleted faster. It also rears the reaction temperature (Ziani and Chaker, 2016). The highest vales belong to the shale gases with N_2 dilution followed by H_2O and CO_2. The total increment rates between 0 and 10 Atm for N_2, H_2O, and CO_2 dilutions are 5.5, 5.3, and 5.3% for Haynesville and 5.6, 5.6, and 5.4% for New Albany in sequence. H_2O addition in the burning air entering into the combustion chamber can be preferred for high operating pressures as well.

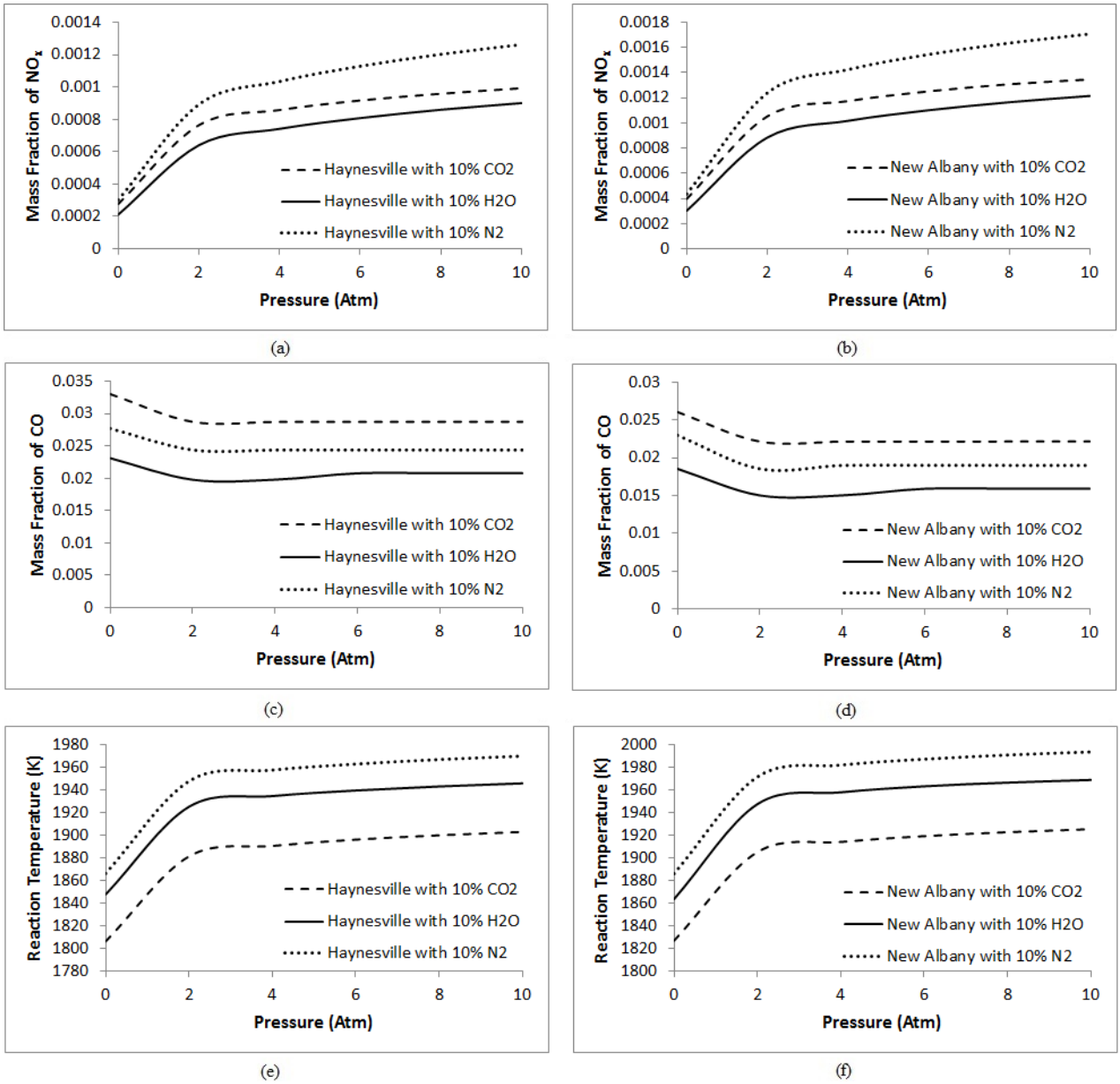

Figure 7. The mass fraction and reaction temperatures of shale gases at different pressures with 10% dilution rates: (a) NO_x mass fractions for Haynesville, (b) NO_x mass fractions for New Albany, (c) CO mass fractions for Haynesville, (d) CO mass fractions for New Albany, (e) Reaction temperatures for Haynesville, and (f) Reaction temperatures for New Albany shale gas.

NO_x mass fractions for Haynesville and New Albany gases with and without additions increases by the rising

wall temperature as represented in Figure 8a, b and c. The enhancing wall temperature reduces heat transfer from the reaction field to outside and advances both the reaction temperature and NO_x. The difference among NO_x values of the combustions with H_2O and the other diluent added airs rises with the lifting wall temperature. The increment rates for NO_x between 300 and 1200 K of the wall temperature with 10% N_2, CO_2, and H_2O dilutions are 235, 259, and 235% for Haynesville and 224, 243, and 226% for New Albany shale gas in turn.

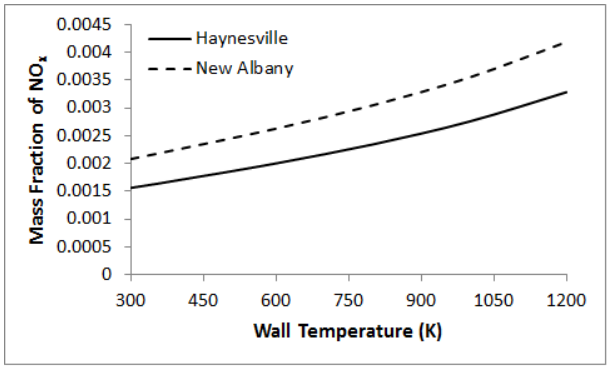

(a)

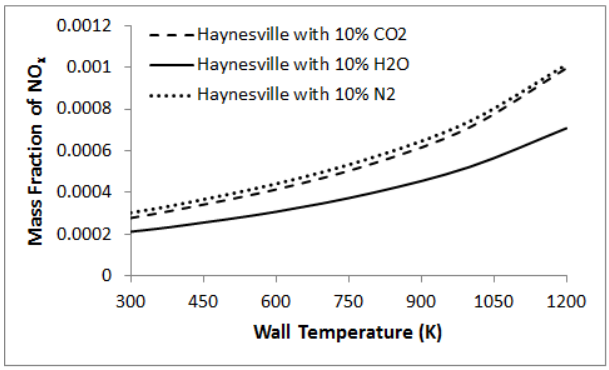

(b)

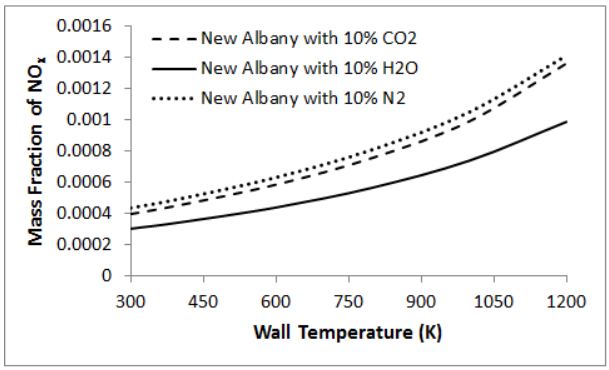

(c)

Figure 8. NO_x mass fractions of shale gases at various wall temperatures: (a) NO_x mass fractions for Haynesville and New Albany without dilution, (b) NO_x mass fraction for Haynesville with 10% dilution rates, (c) NO_x mass fractions for New Albany with 10% dilution rates.

Figure 9a, b, and c present CO mass fractions with and without dilutions at various wall temperatures. The increasing wall temperature raises CO emissions too. The higher temperatures urge CO formation between carbon and oxygen atoms. The rising rates for CO mass fractions between 300 and 1200 K of the wall temperature with 10% CO_2, N_2, and H_2O dilutions are 8.7, 10.9, and 12.4% for Haynesville and 15, 13.1, and 17% for New Albany respectively. The difference among CO emissions of combustions with diluent added airs is constant at the enhancing wall temperature for both gases.

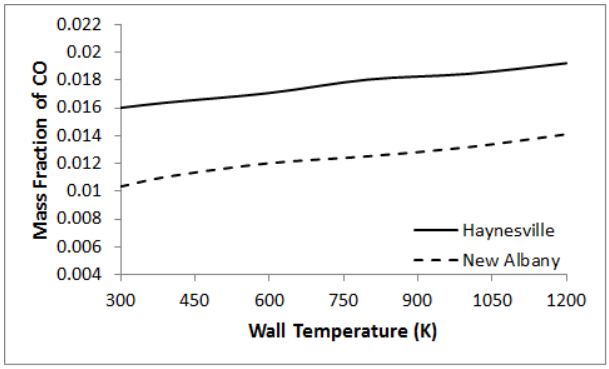

(a)

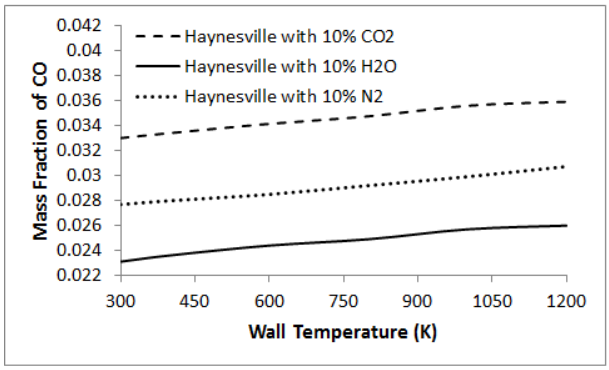

(b)

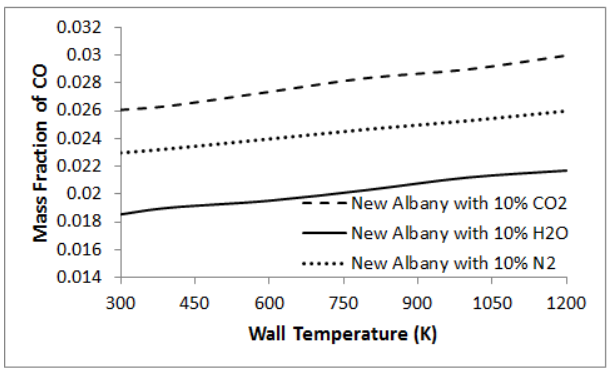

(c)

Figure 9. CO mass fractions of shale gases at various wall temperatures: (a) CO mass fractions for Haynesville and New Albany without dilution, (b) CO mass fraction for Haynesville with 10% dilution rates, (c) CO mass fractions for New Albany with 10% dilution rates.

The rearing wall temperature also uplifts the reaction temperatures for all the shale gases with and without dilutions as depicted in Figure 10a, b, and c. The increasing ratios for the reaction temperatures between 300 and 1200 K of the wall temperature with 10% N_2, H_2O, and CO_2 dilutions are 5.5, 5.4, and 5.8% for Haynesville and 5.5, 5.6, and 5.8% for New Albany in

sequence. The difference among reaction temperatures of the combustions with diluent added airs stays stationary at the enhancing wall temperature for both gases.

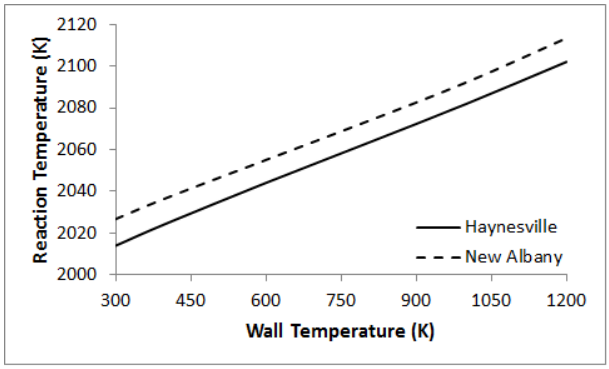

(a)

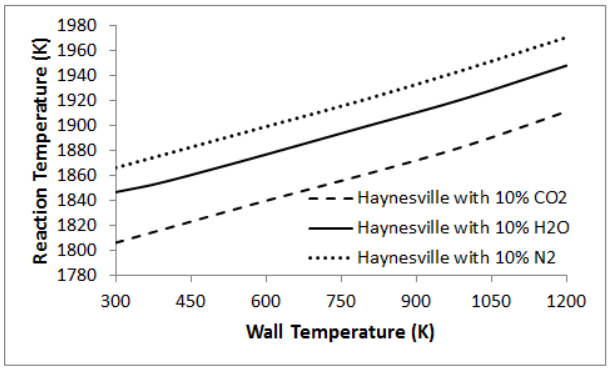

(b)

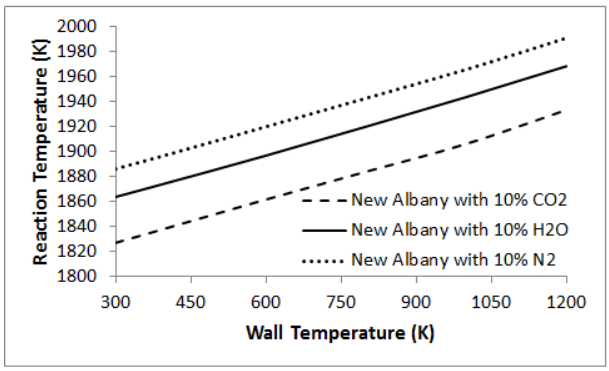

(c)

Figure 10. Reaction temperatures of shale gases at various wall temperatures: (a) Reaction temperatures for Haynesville and New Albany without dilution, (b) Reaction temperature for Haynesville with 10% dilution rates, (c) Reaction temperature for New Albany with 10% dilution rates.

In industrial systems, to reduce the exhaust emissions of environmental pollutants as NO_x, CO, soot, etc. producing at the end of combustion process is used both the procedure of CO_2 and H_2O addition to reactants and pre-heat technique of reactants by exhausted gases (Sabia et al., 2015). Generally, it is seen that the addition of CO_2, H_2O, and N_2 to reactants reduces NO_x with reaction temperature (Zahedi and Yousefi, 2014) and increases CO in exhaust emissions. Moreover, H_2O addition shows the best performance in taking care of NO_x, CO, and reaction temperature as a whole. The increase of pressure raises NO_x (Zahedi and Yousefi, 2014) and reduces CO as expected (Muharam et al., 2015). The rise in wall temperature enhances pollutants emissions and reaction temperature.

CONCLUSION

The characteristics and hazardous emissions of turbulent, non-adiabatic, non-premixed combustions of moist air and shale gases extracted from New Albany and Haynesville fields of United State are numerically investigated in this study. Furthermore, the reaction temperatures and mass fractions of nitrogen oxides and carbon monoxide are determined for various equivalence ratios, pressures, and wall temperatures under the effects of CO_2, H_2O, and N_2 diluents added in the burning air. The following results are obtained:

- The maximum values of mass fractions of NO_x for New Albany and Haynesville shale gas combustion are 0.0021 kg NO_x/kg at ER=1.025 and 0.00158 kg NO_x/kg at ER=1.02 in turn. The difference between NO_x of both shale gas combustions at ER=1 is 25%. The mass fractions of CO rise by raising equivalence ratio. The difference between CO mass fractions is 24.5% at ER=1. The maximum reaction temperatures for New Albany and Haynesville shale gases are 2027 and 2014 K.

- The rising dilution rates generally decrease NO_x values for both shale gases. H_2O dilution is more effective over NO_x to be reduced because of its high heat hold capacity especially. 5% dilution additions of H_2O, CO_2, and N_2 diminish NO_x mass fractions at the rate of 59.1, 51.3, and 51.2% for Haynesville and 57.2, 49.3, and 49.1% for New Albany respectively. The dilution additions increase CO mass fractions for all the shale gas. H_2O dilution has the least effect over CO fractions to enhance. CO_2 has the biggest effect on the reaction temperature to decrease.

- The rearing pressure increases NO_x values for both gases. The highest values for NO_x occur with N_2 dilution followed by CO_2 and H_2O in the decreasing range. On the contrary, the escalating pressure fades CO mass fractions. The advancing pressure causes the reaction temperatures to upsurge. The increment ratios between 0 and 10 Atm for N_2, H_2O, and CO_2 dilutions are 5.5, 5.3, and 5.3% for Haynesville and 5.6, 5.6, and 5.4% for New Albany respectively.

- The ascending wall temperature elevates NO_x values for both gases because of thermal NO_x increment at high reaction temperature. It also boosts both the reaction temperatures and CO mass fractions. The rising rates for the reaction temperatures between 300 and 1200 K of the wall temperature with 10% N_2, H_2O, and CO_2 additions are 5.5, 5.4, and 5.8% for Haynesville and 5.5, 5.6, and 5.8% for New Albany.

ACKNOWLEDGEMENT

The present work is not financially supported by any funding agency.

REFERENCES

Akça H., Ürel G., Karacan C. D., Tuygun N., and Polat E., 2017, The Effect of Carbon Monoxide Poisoning on Platelet Volume in Children, *J Pediatr Emerg Intensive Care Med*, 4, 13-16.

Alberts W. M., 1994, Indoor Air Pollution: NO, NO_2, CO, and CO_2, *J Allergy Clin Immunol*, 94, 289-95.

ANSYS Release 12.0. Tutorial 14.Modeling Species Transport and Gaseous Combustion. 1-46, *ANSYS*, Inc, 2009.

Bilgen, S., and Sarıkaya, İ., 2016, New Horizon in Energy: Shale Gas, *Journal of Natural Gas Science and Engineering*, 35, 637-645.

Bullin K., Krouskop P., and Bryan Research and Engineering Inc. Bryan, Tex., 2008, Composition Variety Complicates Processing Plans for US Shale Gas, *E-book, Based on: Annual Forum, Gas Processors Association, Houston Chapter*, Houston.

Chang Y., Huang R,. Ries R. J., and Masanet E., 2015, Life-Cycle Comparison of Greenhouse Gas Emissions and Water Consumption for Coal and Shale Gas Fired Power Generation in China, *Energy*, 86, 335-343.

Cohen B, and Winkler H., 2014, Greenhouse Gas Emissions from Shale Gas and Coal for Electricity Generation in South Africa, *S Afr J Sci.*, 110 (3/4), 1-5.
Garreton D. and Simonin O., 1994, Aerodynamics of Steady State Combustion Chambers and Furnaces, *In ASCF Ercoftac Cfd Workshop*, Org: EDF Chatou, France.

Hayashi S., Yamada H., Shimodaira K., and Machida T., 1998, NO_x Emissions from Non-Premixed, Direct Fuel Injection Methane Burners at High-Temperature and Elevated Pressure Conditions, *Twenty-Seventh Symposium (International) on Combustion/The Combustion Institute*, 1833-1839.

Hraiech, I., Sautet, J. C., Yon, S., and Mhimid, A., 2015, Combustion of Hythane Diluted with CO_2, *Thermal Science*, 19 (1), 1-10.

Jerzak W., Kuzniaa M., Zajemska M., 2014, The Effect of Adding CO_2 to The Axis of Natural Gas Combustion Fames on CO and NO_x Concentrations in The Combustion Chamber, *Journal of Power Technologies*, 94 (3), 202-210.

McTaggart-Cowan G. P., Wu N., Jin B., Rogak S. N., Davy M. H. and Bushe W. K., 2009, Effects of Fuel Composition on High-Pressure Non-Premixed Natural Gas Combustion, *Combust. Sci. and Tech.*, 181, 397-416.

Muharam, Y., Mahendra, M., Giffari, F., and Kartohardjono, S., 2015, Effects of Injection Temperature and Pressure on Combustion in An Existing Otto Engine using CNG Fuel, *Journal of Environmental Science and Technology*, 8 (1), 25-34.

Lan, Y., Yang, Z., Wang, P., Yan, Y., Zhang, L., and Ran, J., 2019, A Review of Microscopic Seepage Mechanism for Shale Gas Extracted by Supercritical CO2 Flooding, *Fuel*, 238, 412-424.

Ozturk, S., 2018, A Computational Evaluation for Hazardous Emissions of Non-Premixed Shale Gas Combustion, *Journal of Scientific and Engineering Research*, 5 (11), 256-264.

Sabia, P., Lavadera M. L., Giudicianni P., Sorrentino G., Ragucci, R., and Joannon, M., 2015, CO_2 and H_2O Effect on Propane Auto-Ignition Delay Times under Mild Combustion Operative Conditions, *Combustion and Flame*, 162 (3), 533-543.

Silva C. V., Franca F. H. R, and Vielmo H. A., 2007, Analysis of The Turbulent, Non-Premixed Combustion of Natural Gas in A Cylindrical Chamber with and without Thermal Radiation, *Combust. Sci. and Tech.*, 179, 1605-1630.

Vargas A. C., Arrieta A. A., and Arrieta C. E., 2016, Combustion Characteristics of Several Typical Shale Gas Mixtures, *Journal of Natural Gas Science and Engineering*, 33, 296-304.

Wang Q., Chen X., Jha A. N., and Rogers H., 2014, Natural Gas from Shale Formation - The Rvolution, Evidences and Challenges of Shale Gas Revolution in United States, *Renewable and Sustainable Energy Reviews*, 30, 1-28.

Wang, Y., Liao, B., Qiu, L., Wang, D., Xue, Q., 2019, Numerical Simulation of Enhancing Shale Gas Recovery Using Electrical Resistance Heating Method, *International Journal of Heat and Mass Transfer*, 128, 1218-1228.

Zahedi P., and Yousefi K., 2014, Effects of Pressure and Carbon Dioxide, Hydrogen and Nitrogen Concentration on Laminar Burning Velocities and NO Formation of Methane-Air Mixtures, *Journal of Mechanical Science and Technology*, 28 (1), 377-386.

Ziani, L. and Chaker, A., 2016, Ambient Pressure Effect on Non-Premixed Turbulent Combustion of CH_4-H_2 Mixture, *International Journal of Hydrogen Energy*, 41, 11842-11847.

Suat OZTURK received his B. Sc. degree in mechanical engineering in 1996 from Hacettepe University, Turkey. He completed his M. Sc. in electrical and computer engineering at University of Florida in 2001, USA and mechanical engineering at Zonguldak Bülent Ecevit University in 2008, Turkey. He obtained his Ph. D. degree in mechanical engineering at Zonguldak Bülent Ecevit University in 2017, Turkey. He is working as doctor in Department of Electronic and Automation at Zonguldak Vocational School, Zonguldak Bülent Ecevit University, Turkey. His research interests include energy, combustion, computational fluid dynamics, forecasting, economic analysis, composites and mechanical properties.